

A portable laser system for high precision atom interferometry experiments

Malte Schmidt¹, Marco Prevedelli², Antonio Giorgini³, Guglielmo M. Tino³, Achim Peters¹

¹ Humboldt-Universität zu Berlin, Institut für Physik, Hausvogteiplatz 5-7, 10117 Berlin, Germany,
email: malte.schmidt@physik.hu-berlin.de, Tel. +49-30-2093-4941, Fax. +49-30-2093-4718

² Dipartimento di Fisica, Università di Bologna, Via Irnerio 46, 40127 Bologna, Italy

³ Dipartimento di Fisica e Astronomia and LENS, Università di Firenze-INFN, via Sansone 1 Polo Scientifico, 50019 Sesto Fiorentino (Firenze), Italy

Received: date / Revised version: date

Abstract We present a modular rack-mounted laser system for the cooling and manipulation of neutral rubidium atoms which has been developed for the portable gravimeter GAIN, an atom interferometer that will be capable of performing high precision gravity measurements directly at sites of geophysical interest. This laser system is designed to be compact, mobile and robust, yet it still offers improvements over many conventional laboratory-based laser systems. Our system is contained in a standard 19" rack and emits light at five different wavelengths simultaneously on up to 12 fibre ports at a total output power of 800 mW. These wavelengths can be changed and switched between ports in less than a microsecond. The setup includes two phase-locked Raman lasers with a phase noise spectral density of less than $1 \mu\text{rad}/\text{Hz}^{1/2}$ in the frequency range in which our gravimeter is most sensitive to noise. We characterize this laser system and evaluate the performance limits it imposes on an interferometer.

1 Introduction

Since first experimental demonstrations in 1991 [1,2,3,4], atom interferometry has developed into a powerful tool for the ultra precise measurement of accelerations and rotations. It is now used in various laboratories for experiments in the fields of fundamental physics [5] and metrology [6,7,8]. Most of these setups, however, are laboratory-bound and cannot be used for field research such as gravity mapping, geophysics, seismology or navigation, even though the accuracy of atom interferometers could substantially exceed that of classical gravimeters [9]. Our transportable high-precision gravimeter will therefore open up new possibilities in all of these fields

[10] and might in future versions also be used on satellite missions [11,12].

The working principle of a gravimetric atom interferometer has been described in detail elsewhere [6,13]. In short: An ensemble of laser-cooled neutral atoms (in our case Rubidium 87) is prepared in a 3D Magneto-Optical Trap (MOT), further cooled in optical molasses, and launched upwards. During their parabolic flight, the atoms are subjected to three pulses from counterpropagating laser beams, thereby inducing Raman transitions that transfer them between the two hyperfine ground states via a stimulated Raman process. The sequence consists of one $\frac{\pi}{2}$ -, one π -, and finally another $\frac{\pi}{2}$ -pulse, which constitute an atom optic beam splitter, mirror and recombiner, respectively. Thereby the atomic wave packet is split into two parts that travel on different trajectories due to momentum transfer from the photons. At the output of the atom interferometer the transition probability P from one hyperfine state to the other is given by $P = \frac{1}{2}(1 + C \cos \Delta\Phi)$, where $\Delta\Phi$ is the accumulated phase difference between wave packets and C the contrast of the measurement. This includes the acceleration contribution of $\Delta\Phi_g = k_{\text{eff}} g T^2$ with T being the time between two consecutive Raman pulses, k_{eff} the sum of the Raman laser wavenumbers and g the local gravitational acceleration.

2 Concept

Naturally, the laser system for a mobile atom interferometer has to be mobile and compact as well. Standard laser systems for cold atom experiments, however, are not only quite complex, but also can rarely endure significant mechanical vibrations, thermal fluctuations of even a few degrees or electromagnetic noise, without losing laser frequency locks or a significant decrease in optical power output. A first step in solving these problems was the redesign from scratch of almost all optical mounts,

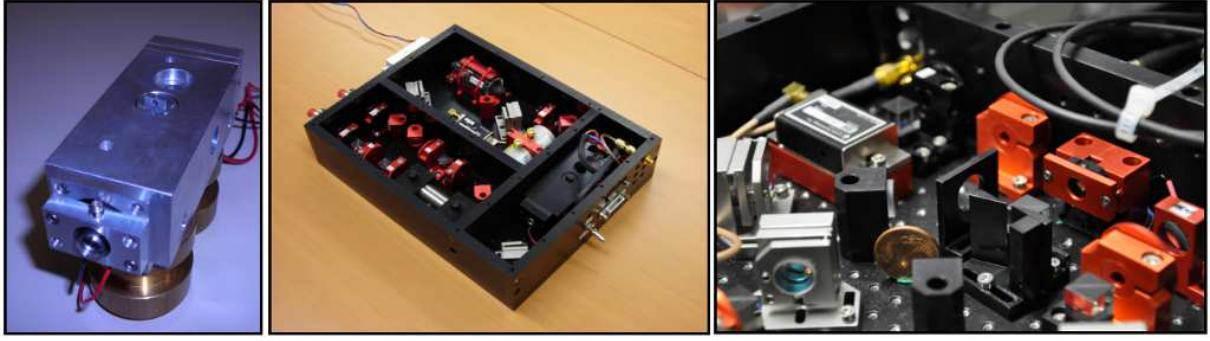


Fig. 1 Custom-made miniaturized optical mounts. Beam height for all optics is 20 mm, round optical components have a diameter of 0.5". Left to right: External Cavity Diode Laser, Reference laser module, Raman laser module detail with a 5-Eurocent coin ($d = 21$ mm) as reference

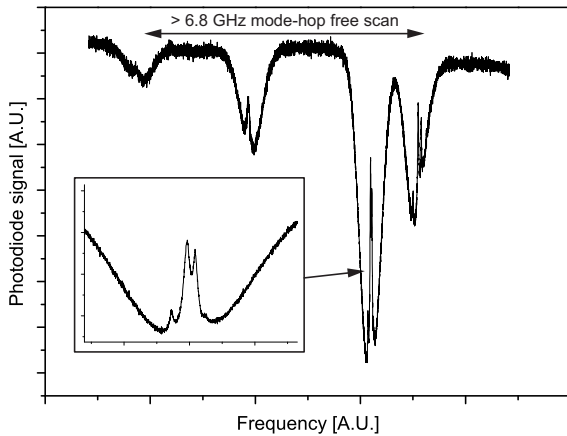


Fig. 2 Mode-hop free scan over the complete ^{87}Rb D2 line spectrum using one of our ECDLs. Insert: ^{85}Rb $F=3 \rightarrow F'$ lines that we use to stabilise the laser.

as standard laboratory equipment rarely offers sufficient mechanical stability and is in most cases simply too large for our purposes (Figure 1). Some of these mount designs are adapted from the QUANTUS drop tower project [14] and have proven their stability even under extreme accelerations of up to $50 g$. We further improved ruggedness by containing all optics in four closed, compact modules with 1 cm thick walls and a beam height of 20 mm. Light is transferred between the modules by means of polarisation maintaining optical fibres. Except for the reference laser, which is even smaller, each module's base area is 42 by 42 cm with a height of a few centimeters. The base plate of two of these modules is a custom made honeycomb breadboard with a 1 cm thread grid which provides stability as well as flexibility for possible future modifications. The other two modules use 25 mm thick aluminum slabs as base plates with the four walls and two additional divider walls mounted in a force-fit for optimal stiffness. Fibre and electrical connections are mounted on the walls of each module, the total height of each module varies between 75 and 105 mm.

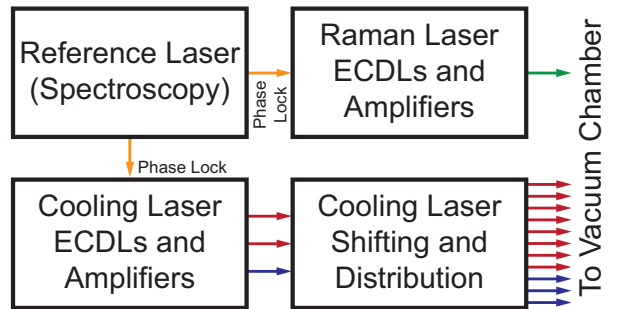


Fig. 3 Modular concept of our laser system

As laser sources we have built compact external cavity diode lasers (ECDL). They include an interference filter as a wavelength selector that is one order of magnitude less sensitive to angular misadjustments than gratings found in conventional ECDL configurations which makes it suitable for our application. These ECDLs have been adapted from a design developed at SYRTE [15]. The output power is up to 50 mW and the intrinsic linewidth less than 10 kHz. Control of the laser frequency is achieved by tuning of either the laser diode current or the cavity length (via a piezo). Applied separately, the mode-hop-free tuning range is limited to 200 MHz or 2 GHz, respectively. However, by controlling both parameters simultaneously at a fixed gain ratio, a mode-hop free tuning range of about 9 GHz and thereby over more than the complete ^{87}Rb D2 line was achieved (Figure 2).

To provide the various optical frequencies required to operate an atomic fountain interferometer and yet still maintain sufficient flexibility for future enhancements like quasi-continuous operation (many clouds of atoms in flight at the same time), a total of five ECDLs is employed. They are organized in four distinct modules: one reference laser module, two cooling laser modules and one Raman laser module (Figure 3).

The modules are mounted in a standard 19" electronics rack that has been modified to include a passive vibration isolation and is dimensioned such that it can fit through standard doors and is thereby easily transportable to different locations (Figure 4). For

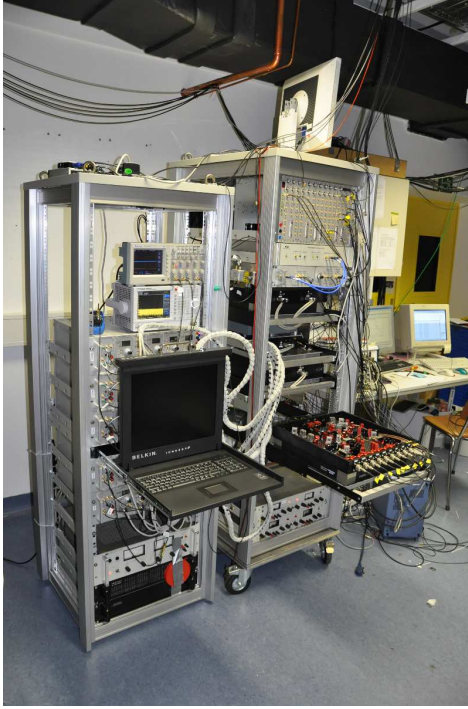


Fig. 4 Photograph of laser system, cooling module 2 extended on telescopic rails. In addition to the complete laser system, these two racks also contain the gravimeter’s computer, power supplies, emergency backup batteries, control electronics and diagnostic equipment

easy access, the laser modules are mounted on telescopic rails. The complete laser system and its control electronics could easily be mounted in just one rack – we chose, however, to also include other gravimeter electronics such as computer control, a backup power system, power supplies and diagnostic equipment which made a second rack necessary and enabled us to move mechanically noisy equipment (i.e. anything that includes cooling fans) away from the optics.

The dimensions of the complete system are $177 \times 60 \times 60 \text{ cm}^3$ (computer and control electronics rack) plus $194 \times 80 \times 60 \text{ cm}^3$ (laser rack), adding up to a total volume of 1.6 m^3 . Power consumption is less than 1 kW.

3 Reference Laser

The reference laser module houses an ECDL that is stabilized 40 MHz below the ^{85}Rb $F=3 \rightarrow F'=4$ transition by modulation transfer spectroscopy [16]. Two feedback paths are employed: A fast control path controls the laser diode current and a slow control path controls both current as well as cavity length at the same gain ratio used for 9 GHz mode-hop-free tuning. This way, the laser stays locked over days at its required frequency even when submitted to temperature drifts or mechanical vibrations. By selecting pumping beam intensity and diameter carefully, we reached a regime in

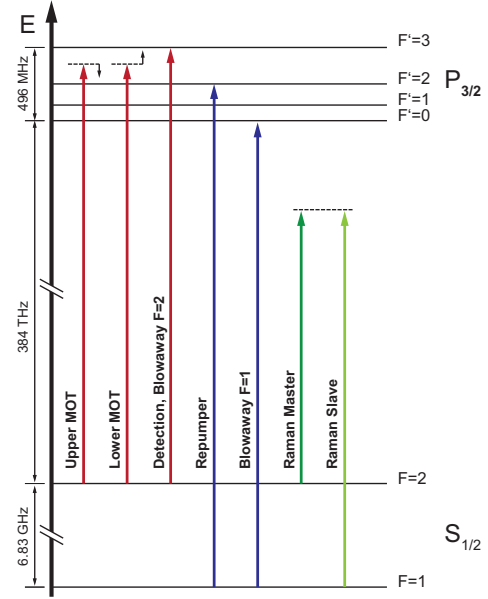


Fig. 5 ^{87}Rb D2 level scheme and laser frequencies required in our setup

which the atoms are pumped quickly into the desired internal states, thereby achieving a locking bandwidth of approximately 300 kHz.

4 Cooling Laser System

An atomic fountain setup requires a variety of optical frequencies in order to trap, cool, launch, select and detect the atoms, as can be seen in Figure 5. In our vacuum chamber, we capture the atoms in a Magneto-Optical Trap (MOT). Since the atom interferometer’s precision scales with the square root of both the repetition rate and the number of atoms, we aim to trap as many atoms as possible as quickly as possible. To achieve this, we use a large MOT volume (beam diameter 35 mm) at high laser power ($> 300 \text{ mW}$). In order to launch the atoms, both upper and lower MOT beams have to be detuned with respect to each other to achieve a moving molasses configuration [17]. Additionally, a repumper is required, as well as blow-away and detection light in both $F=1 \rightarrow F'$ and $F=2 \rightarrow F'$ frequency classes. A total of 11 separate fibre output ports at different laser powers and frequencies is required for full functionality.

Due to the large hyperfine ground splitting of 6835 MHz, light from the $F=1 \rightarrow F'$ frequency class cannot easily (or with high efficiency) be shifted to $F=2 \rightarrow F'$ by means of acousto-optical modulators. Hence, we employ two ECDLs mounted in the first cooling laser module, one for each frequency class. For frequency stabilization, light from each ECDL is overlapped with light from our reference laser on a fast photodiode resulting in beat frequencies of about 5080 MHz and 1000 MHz, respectively. The signals frequencies are subsequently divided down to about 19.8 MHz (factor 256) and 100 MHz (factor

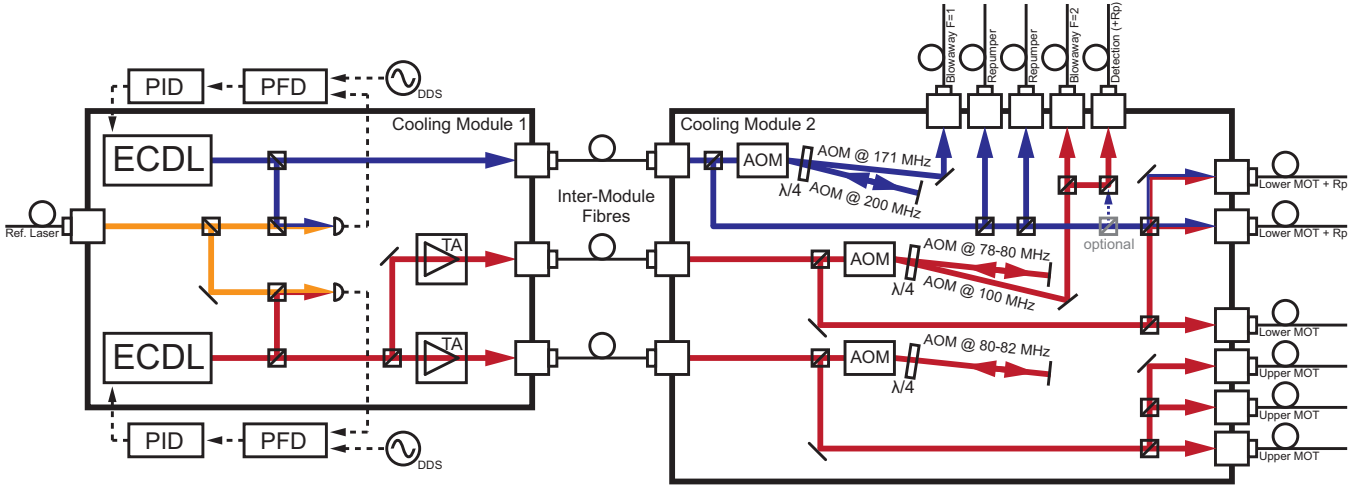


Fig. 6 Layout of Cooling laser modules

10), respectively. Comparing the resulting signal's zero-crossings to those of a stable Direct Digital Synthesizer (DDS) reference frequency in a Hittite HMC440QS16G digital phase-frequency detector (PFD) gives an error signal that we use to phase-lock the beat signal onto the DDS reference at a bandwidth of 200 kHz. This setup enables us to reach any desired laser frequency simply by changing the DDS frequency. The $F=2 \rightarrow F'$ laser light is split into two halves, each of which is amplified to 1 Watt by a tapered amplifier. Both of these amplified beams as well as the $F=1 \rightarrow F'$ light is mode-cleaned by optical fibres and fed into the second cooling module.

There the light is frequency shifted and switched using acousto-optical modulators (AOMs), one for each of these three beams. This enables separate frequency and switching control of upper MOT, lower MOT and repumper beams. Not all eleven output ports will have to be used simultaneously, as for instance blow-away beams and MOT light are not required at the same time. By changing the AOMs' frequencies, the first order diffraction beam angle varies slightly. We make use of this effect and hit different mirrors at different AOM frequencies, one of which directs the light into one fibre, the other one reflects the light back into the AOM for a double pass configuration. Effectively, this enables us to switch between different fibre outputs at different laser frequencies within less than a microsecond without losing any light power at ports that are not in use at any given moment. To avoid unwanted scattered light, additional mechanical shutters (shutting time 1-2 ms) are used at each of the eleven output ports. A schematic of this setup is shown in Figure 6, the total output power of this system in MOT configuration is six times 60 mW cooling light plus 5 mW repumper light.

5 Raman Lasers

In order to induce an optical Raman transition between the hyperfine ground states of the atoms, a pair of two lasers with a fixed phase relation and a frequency difference of 6.835 GHz (the ^{87}Rb ground state hyperfine splitting) is required to drive the two-photon transition via an intermediate level, as seen in Figure 5. Any phase noise between the Raman lasers will be imprinted onto the atoms and will therefore directly limit the gravimeter's sensitivity. In this section, we will describe our Raman laser system and its performance.

We employ two ECDLs (Figure 7) which emit light that is amplified to 1 Watt using Tapered Amplifiers and then overlapped. Rubidium vapour cells are employed to suppress unwanted amplified spontaneous emissions on atomic resonances. An AOM is used for fast switching and pulse-shaping of the Raman pulses. Identical pulse-shaping on both laser beams is ensured by an intra-module fibre where the light is mode-cleaned before entering the AOM. The Raman master laser ECDL is phase-locked to the reference laser using a setup similar to the one employed in the cooling laser system, however the PFD we use here is an Analog Devices ADF4108.

The Raman slave laser ECDL is stabilised in frequency and phase in respect to the Raman master laser. For this phase lock between the two ECDLs, light from both lasers is overlapped on a fast photodiode that is placed behind the intra-module fibre so that all noise sources that are not common to both beams (i.e. anything before overlapping and mode-cleaning done by the fibre) can be compensated for by the phase lock. The resulting beat signal of 6835 MHz is mixed down using a stable 6735 MHz reference. The resulting 100 MHz signal is phase-locked onto a DDS reference frequency using a Motorola MC100EP140 PFD. However, in this case we aim for locking bandwidths of some MHz. To overcome bandwidth limitations and thereby residual phase noise imposed by long cables and the laser diode current

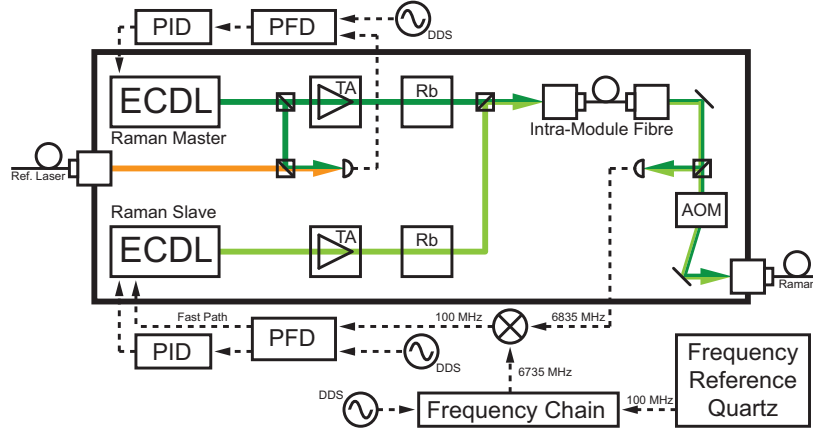


Fig. 7 Layout of Raman laser module

controller's response time, an additional high frequency path is employed that modulates the ECDL laser diode's current directly via a small signal N-channel FET as a voltage to current converter and a lag-lead compensation network.

The 6735 MHz mixing-down frequency is generated by a frequency chain that employs an ultra-low noise 100 MHz quartz (Wenzel Blue Top), which is multiplied to 6800 MHz and is then used to lock a Dielectric Resonator Oscillator (DRO) to 6735 MHz – this frequency chain is identical to the one described in [9].

By beating the mixed-down signal with the 100 MHz reference, we measured the phase noise spectral density of this optical phase lock loop (OPLL) independent of noise in the reference signal (Figure 8). Between 100 Hz and 60 kHz, where our interferometer is most sensitive to noise (as shown in section 6), it largely stays below a level of -120 dB rad^2/Hz ($1 \mu\text{rad}/\text{Hz}^{1/2}$). The achieved closed-loop bandwidth is slightly above 4 MHz. Also shown in Figure 8 is the performance of the frequency chain and that of the reference quartz as described and characterized in [9]. To reduce low-frequency noise further, we will lock the quartz at a low bandwidth onto a 10 MHz GPS reference, however this system is not in place yet.

6 Gravimeter sensitivity

In this section, we will calculate the limit to our gravimeter's sensitivity due to phase noise from the Raman laser system. Of course, these are not the only noise sources in our gravimeter, as we are amongst others sensitive to mechanical vibrations and detection noise. These noise sources will be evaluated in future publications. In a setup like ours, the precision $\frac{\Delta g}{g}$ with which we are able to measure local g in a single measurement is limited by the phase uncertainty $\Delta\Phi$ as follows:

$$\frac{\Delta g}{g} = \frac{\Delta\Phi}{k_{\text{eff}} T^2 g} \quad (1)$$

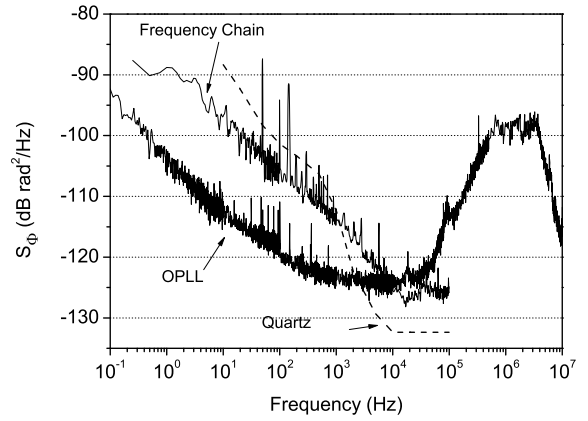


Fig. 8 Phase noise spectral density for Raman laser OPLL, frequency chain (data from [9]) and quartz at 6.8 GHz

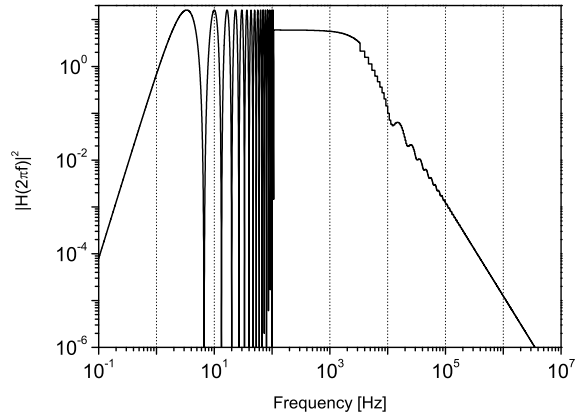


Fig. 9 $|H(2\pi f)|^2$ calculated for $T=150$ ms and $\tau=100 \mu\text{s}$, averaged after 16 oscillations

The contribution of the Raman laser's power spectral density S_Φ affects $\Delta\Phi$ via a transfer, or weighting function, $|H(\omega)|^2$, i.e. $\Delta\Phi$ can be evaluated as

$$\Delta\Phi^2 = \int_0^\infty |H(2\pi f)|^2 S_\Phi(f) df \quad (2)$$

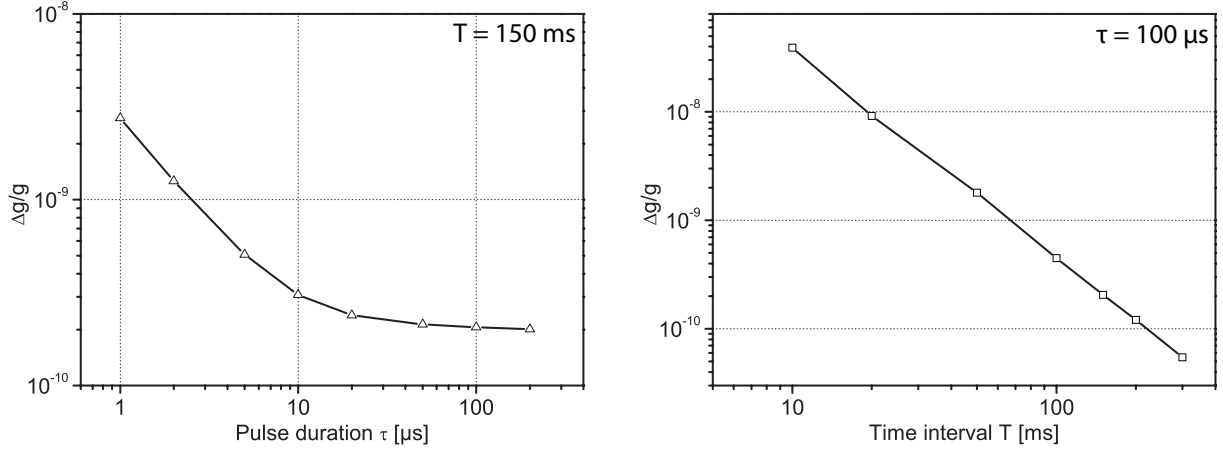


Fig. 10 Sensitivity limit given by Raman laser phase noise for various values of τ and T

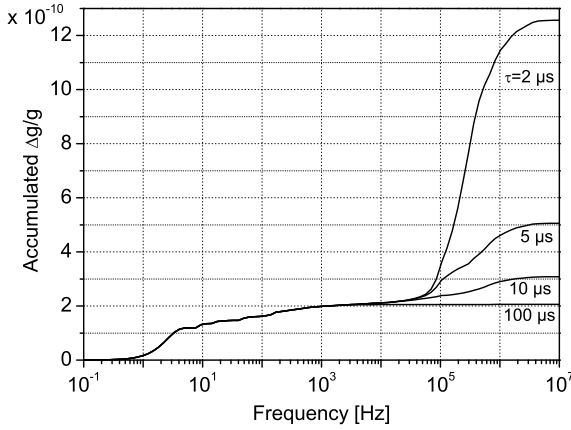


Fig. 11 $\Delta g/g$ as a function of the upper limit in the Raman laser power spectral density integration, displayed for various pulse lengths τ . $T = 150$ ms is held constant.

In our setup we employ three Raman pulses: One $\frac{\pi}{2}$ -pulse, one π -pulse, and finally another $\frac{\pi}{2}$ -pulse. Assuming square Raman pulses of duration τ , separated by time T , the explicit form for $|H(\omega)|^2$ as derived in [18] is

$$|H(\omega)|^2 = \left| -\frac{4\Omega\omega}{\omega^2 - \Omega^2} \times \sin\left(\omega\frac{T+2\tau}{2}\right) \times \left[\cos\left(\omega\frac{T+2\tau}{2}\right) + \frac{\Omega}{\omega} \times \sin\left(\omega\frac{T}{2}\right) \right] \right|^2 \quad (3)$$

with $\Omega = \pi/2\tau_R$ being the Rabi oscillation frequency of the Raman transition. Due to a highly oscillatory behavior of $H(\omega)$, however, after the 16th oscillation only the average value is calculated (Figure 9) in order to avoid aliasing effects due to our limited data point spacing at higher frequencies. Also of note is the band pass filter behavior of $|H(2\pi f)|^2$ whose effective lower cut-off frequency scales with T^{-1} , whereas the upper cutoff frequency scales with τ^{-1} .

Calculating the root-mean-square of our three noise spectra (OPLL, frequency chain, quartz) and multiplying it with $|H(2\pi f)|^2$, we can evaluate the sensitivity

limit of our gravimeter. Integrating over the complete frequency spectrum, we obtain our limits for $\Delta\Phi^2$ and consequently for $\frac{\Delta g}{g}$. Assuming standard operating parameters for our gravimeter of $T=150$ ms and $\tau=100$ μ s, our single-shot sensitivity will be limited to $\frac{\Delta g}{g} = 1.93 \times 10^{-10}$ by Raman laser phase noise.

For different T and τ , the band pass behavior of the weighting function changes and so does our sensitivity to certain phase noise frequencies. The resulting sensitivity limits are shown in Figure 10. To illustrate which frequencies are the dominant contributors to these limit calculations, we have plotted an accumulation integral for different pulse lengths (Figure 11). In this diagram, $\frac{\Delta g}{g}$ is plotted against x in $\Delta\Phi^2 = \int_0^x |H(2\pi f)|^2 S_\Phi(f) df$. As can be seen, our 4 MHz servo bump (see Figure 8) does not significantly contribute to the overall gravimeter sensitivity at long pulse lengths τ , at shorter pulse lengths, however, the noise spectrum in the MHz range becomes a dominating factor. A variation of pulse spacing T instead of τ does not notably alter our sensitivity to low frequency phase noise, as the low-frequency part of the area under the $|H(2\pi f)|^2 S_\Phi(f)$ curve remains insignificant. However, Δg scales with T^{-2} , so we still want to keep T as long as possible in our apparatus (see Figure 10).

7 Conclusion

We have designed and built a laser system for atom interferometry applications that is mobile and robust, yet still offers improvements over many conventional laboratory-based systems. This system enables us to operate a highly precise atom interferometer outside of standard laboratory conditions and thereby opens up new possibilities for geophysical gravity measurements.

Acknowledgements

This work is supported by the European Commission (FINAQS, Contr. No. 012986-2 NEST), by the ESA (SAI, Contr. No. 20578/07/NL/VJ) and by the ESF/DFG (EuroQuasarIQS project). We further thank LNE-SYRTE for design and construction of the frequency chain.

References

1. O. Carnal and J. Mlynek, *Phys. Rev. Lett.* **66**, 2689 (1991).
2. F. Riehle, T. Kisters, A. Witte, J. Helmcke and C. Borde, *Phys. Rev. Lett.* **67**, 177 (1991).
3. D. Keith, C. Ekstrom, Q. Turchette and D. Pritchard, *Phys. Rev. Lett.* **66**, 2693 (1991).
4. M. Kasevich and S. Chu, *Appl. Phys. B* **54**, 321 (1992).
5. S. Dimopoulos, P. W. Graham, J. M. Hogan and M. A. Kasevich, *Phys. Rev. D* **78**, p. 042003 (2008).
6. A. Peters, K. Chung and S. Chu, *Metrologia* **38**, 25 (2001).
7. T. Gustavson, A. Landragin and M. Kasevich, *Class. Quantum Grav.* **17**, 2385 (2000).
8. M. Snadden, J. McGuirk, P. Bouyer, K. Haritos and M. Kasevich, *Phys. Rev. Lett.* **81**, 971 (1998).
9. J. Le Gouet, T. E. Mehlstaebler, J. Kim, S. Merlet, A. Clairon, A. Landragin and F. P. Dos Santos, *Appl. Phys. B* **92**, 133 (2008).
10. M. de Angelis, A. Bertoldi, L. Cacciapuoti, A. Giorgini, G. Lamporesi, M. Prevedelli, G. Saccorotti, F. Sorrentino and G. M. Tino, *Meas. Sci. Technol.* **20**, p. 022001 (2009).
11. G. M. Tino, L. Cacciapuoti, K. Bongs, C. J. Borde, P. Bouyer, H. Dittus, W. Ertmer, A. Goerlitz, M. Inguscio, A. Landragin, P. Lemonde, C. Lammerzahl, A. Peters, E. Rasel, J. Reichel, C. Salomon, S. Schiller, W. Schleich, K. Sengstock, U. Sterr and M. Wilkens, *Nucl. Phys. B* **166**, 159 (2007).
12. S. G. Turyshev, U. E. Israelsson, M. Shao, N. Yu, A. Kuzenko, E. L. Wright, C. W. F. Everitt, M. Kasevich, J. A. Lipa, J. C. Mester, R. D. Reasenber, R. L. Walsworth, N. Ashby, H. Gould and H. J. Paik, *Int. J. Mod. Phys. D* **16**, 1879 (2007).
13. B. Dubetsky and M. A. Kasevich, *Phys. Rev. A* **74**, p. 023615 (2006).
14. A. Vogel, M. Schmidt, K. Sengstock, K. Bongs, W. Lewoczko, T. Schuldt, A. Peters, T. Van Zoest, W. Ertmer, E. Rasel, T. Steinmetz, J. Reichel, T. Koenemann, W. Brinkmann, E. Goeklue, C. Laemmerzahl, H. J. Dittus, G. Nandi, W. P. Schleich and R. Walser, *Appl. Phys. B* **84**, 663 (2006).
15. X. Baillard, A. Gauguier, S. Bize, P. Lemonde, P. Laurent, A. Clairon and P. Rosenbusch, *Opt. Comm.* **266**, 609 (2006).
16. J. Supplee, E. Whittaker and W. Lentz, *Appl. Opt.* **33**, 6294 (1994).
17. M. Kasevich, D. Weiss, E. Riis, K. Moler, S. Kasapi and S. Chu, *Phys. Rev. Lett.* **66**, 2297 (1991).
18. P. Cheinet, B. Canuel, F. P. Dos Santos, A. Gauguier, F. Yver-Leduc and A. Landragin, *IEEE Trans. Instrum. Meas.* **57**, 1141 (2008).